ELSEVIER

Polymer 43 (2002) 5679–5691

polymer

www.elsevier.com/locate/polymer

Ultimate mechanical properties of rubber toughened semicrystalline PET at room temperature

Wendy Loyens, Gabriël Groeninckx*

Laboratory of Macromolecular Structural Chemistry, Department of Chemistry, Katholieke Universiteit Leuven (KULeuven), Celestijnenlaan 200F, B-3001 Heverlee, Belgium

Received 14 February 2002; received in revised form 5 July 2002; accepted 9 July 2002

Abstract

A comparative fundamental study was performed regarding the notched impact toughening performance of various rubber modified semicrystalline polyethylene terephthalate (PET) systems. Various modifiers with and without functional groups were evaluated: ethylene-*co*-propylene rubber (EPR), maleic anhydride grafted EPR (EPR-*g*-MA), glycidyl methacrylate grafted EPR (EPR-*g*-GMA*x*) and ethylene–glycidyl methacrylate copolymers (E–GMA*x*). Both binary and ternary blends (consisting of a preblend of EPR and a functionalised modifier) were examined. The most effective toughening route for PET is provided by dispersing a preblend of EPR and a low amount of E–GMA*x*. A minimum dispersed phase concentration of 30 wt% is needed to obtain a pronounced improvement of the impact strength and to induce a brittle–ductile transition of the fracture mode. The impact behaviour of the rubber toughened PET is primarily controlled by the morphological characteristics, i.e. the interparticle distance. An equal critical interparticle distance (IDc) of 0.1 μm was established experimentally for the different GMA compatibilised systems. This IDc is found to be independent of the amount of GMA functionalities present, the way of incorporation in the chain (grafting or copolymerisation) and the nature of the compatibiliser. The ternary PET/(EPR/E–GMA8) blends provided the best ultimate mechanical properties, displaying highly (15-fold) increased impact strengths and reasonable elongations at break.

Keywords: Rubber toughening; Semicrystalline polyethylene terephthalate; Glycidyl methacrylate

1. Introduction

In the packaging industry, polyethylene terephthalate (PET) shows a consistently growing market share. This is mainly due to its excellent chemical resistance and good optical and barrier properties. The improved mechanical properties arising from biaxial stretching during the blow moulding process have added greatly to its use. However, this biaxial orientation cannot be obtained using other processing methods, like sheet extrusion or compression moulding. Semicrystalline engineering thermoplastics (e.g. polyesters) generally display a high craze stress and will therefore preferentially deform by shear yielding [1,2]. However, the presence of a notch is often detrimental and results in a brittle failure, limiting the applicability of these notch sensitive polymers. Rubber modification provides an effective method for increasing the fracture toughness and inducing a brittle/tough transition of the fracture mode [1–6]. The function of the dispersed rubber particles is two-fold [1,4]. They need to generate a local stress concentration. Secondly, they need to void (cavitate/debond) in order to alter the stress state in the surrounding matrix material and allow an overall deformation mechanism to take place. The ultimate mechanical properties depend strongly on the blend characteristics and its constituting components. It is generally known that the blend morphology plays a very important role in the toughening concept [1,7–12]. The most important factors characterising the phase morphology are the rubber type and concentration, the rubber particle size, the interfacial effects and the matrix molar mass [2,10–22].

Most studies have been focussed on PBT (polybutylene terephthalate) rather than PET. It can be anticipated that the same general aspects of toughening will apply. However, the structural differences between both materials will inevitably result in differences regarding their overall physical behaviour, i.e. processing temperatures, compatibilisation

* Corresponding author. Tel.: +32-1632-7441; fax: +32-1632-7990.
E-mail address: gabriel.groeninckx@chem.kuleuven.ac.be (G. Groeninckx).

0032-3861/02/$ - see front matter
PII: S0032-3861(02)00472-X

efficiency, crystallisation kinetics. Several different routes have been explored for the toughening of polyesters with varying success: core–shell modifiers [23–26], ABS (acrylonitrile–butadiene–styrene) with or without functionalisation [27–30] and several functionalised elastomers [7,8,31–36].

The addition of elastomers results in an improved overall toughness, provided that the rubber phase is finely dispersed, on the submicron level, in the PET matrix. Since there usually exists a high interfacial tension between the polar polyesters and the apolar elastomers, the use of reactive compatibilisation becomes necessary in order to obtain the desired dispersed phase morphology. In literature, different types of elastomers and functional groups have been explored. Ethylene–propylene rubber grafted with maleic anhydride (EPR-*g*-MA) and ethylene–propylene diene rubber grafted with maleic anhydride (EPDM-*g*-MA) are two of the most frequently added components. The use of EPR-*g*-MA for the toughening of PET was reported by Wu [37] and Penco et al. [33]. Cecere et al. [31] and Kanai et al. [7] used EPR-*g*-MA to toughen PBT. Kanai et al. [7] investigated the influence of the amount of grafted MA and the molar mass of PBT. They established a correlation between the impact strength and the critical interparticle distance (IDc), which was found to be independent of the matrix viscosity, the amount of adhesion and the rubber content.

From literature and our earlier results [38] it is known that very effective compatibilisation of PET/elastomer blends can be obtained in the presence of glycidyl methacrylate (GMA) functional groups. Hert [36] and Akkapeddi et al. [32] have used several GMA holding co- and terpolymers to improve the impact toughness of PET and PBT, respectively. Paul and his coworkers [28–30] have synthesised a terpolymer of methyl methacrylate–glycidyl methacrylate–ethyl acrylate (MGE) to compatibilise PBT/ABS blends. The resulting finer morphologies led to improved impact strengths and a low temperature toughness whereby a minimum of 30 wt% of ABS was needed.

In our previous publication [38], we already reported on the morphology development and rheological behaviour of various PET/(elastomer/compatibiliser) blends with EPR as the basic elastomeric component. The effect of the following compatibilising agents has been explored: EPR-*g*-MA, ethylene–glycidyl methacrylate copolymers (E–GMA having 8 or 12 wt% of GMA) and home-made EPR-*g*-GMA*x* (x = wt% of grafted GMA) grades. The present paper now concentrates on a comparative, fundamental study of the toughening efficiency of these different rubber modified systems in order to determine the most effective toughening route for semicrystalline PET. When developing a toughening route, it is important to have a good idea about the influence of the various parameters controlling the toughening process. The influence of the morphological blend characteristics and the elastomer type on the notched Izod impact response will be investigated. A possible direct correlation between the impact response and the blend morphology will be explored.

2. Experimental

2.1. Materials

The PET compound used was a grade from Shell Chemical ($M_n = 29\,500$ g/mol and $\rho = 1.40$ g/cm^3) with trade name Caripak G82. The basic, non-reactive elastomer, EPR, with trade name Vistalon 805 (E/P ratio = 78/22, $\rho = 0.86$ g/cm^3) was kindly supplied by Exxon Chemical. The maleic anhydride grafted EPR (Exxelor VA 1801 from Exxon) contained 0.6 wt% of MA (E/P ratio = 75/25, $\rho = 0.86$ g/cm^3). Two different types of E–GMA copolymers were used; E–GMA8 (8 wt% GMA, MFI (190 °C, 2.16 kg) = 5 g/10 min) was supplied by Elf Atochem with trade name Lotader AX 8440 and E–GMA12 (12 wt% GMA, MFI = 3 g/10 min) was Igetabond E from Sumitomo. Besides these commercially available compatibilisers, use was also made of home-made EPR-*g*-GMA*x* grades. The radical grafting preparation procedure has been addressed in a previous publication [38]. Two different types of the home-made grafted EPR-*g*-GMA*x* grades will be investigated, namely EPR-*g*-GMA2.0 and EPR-*g*-GMA1.5, respectively, containing 2.0 and 1.5 wt% of grafted GMA.

2.2. Blend preparation and compounding

Prior to blending, all materials were dried overnight under vacuum, PET at 120 °C and the compatibilisers at 70 °C. Before blending with PET, EPR and the compatibiliser were preblended at different ratios, eventually resulting in the smallest dispersed phase sizes. The preblending was done on a Haake Rheocord 9000 batch mixer using a small mixing chamber of 69 cc at a temperature of 180 °C and a screw speed of 50 rpm during 5 min. These preblends were pelletised and then mixed together with the PET matrix to give rise to ternary blend systems. Each rubber and compatibiliser component was also blended separately with PET to obtain binary blends. The compounding of the binary and ternary blends was performed on the Haake batch mixer using a mixing chamber of 300 cc at a temperature of 280 °C and a screw speed of 50 rpm during a total mixing time of 10 min. The blending conditions were chosen by variation of rotor speed, blending temperature and mixing time. The compositions of the ternary PET/(elastomer/compatibiliser) blends are based on a constant weight concentration of the dispersed phase but with a changing ratio (elastomer/compatibiliser) of the two dispersed phase components.

After mixing, the blends were dried at 120 °C before being compression moulded into plaques whose dimensions

depended on the test method used. The blends were firstly molten in a hydraulic press (Carver) at 280 °C and held under pressure for 90 s. The mould was then transferred directly into a second press held at a temperature of 180 °C. The complete moulding set up was kept under pressure during 5 min. After removal, the plaques were left to cool to room temperature. This procedure was applied in order to control the overall crystallisation conditions. The compression moulding steps were carried out carefully in order to obtain the same treatment for every system.

2.3. Morphological analysis

The blend phase morphology was investigated with scanning electron microscopy on small pieces taken from the compression moulded samples at various sites. The samples were smoothed on a Leica Ultracut UCT cryomicrotome at − 100 °C and afterwards etched in *m*-xylene at 105 °C during 5 h to remove the minor phase. After gold sputtering the surfaces were examined with a Philips XL-20 scanning electron microscope. To quantitatively analyse the morphology, several micrographs of each sample were taken for a total of at least 600 particles. Leica Qwin image analysis software was used to determine the main morphological characteristics.

2.4. Mechanical properties

Notched Izod impact tests were performed at room temperature according to ISO-180 on a Zwick 5110 apparatus. The samples with dimensions $63 \times 10 \times 4$ mm^3 were machine-cut from the compression moulded plaques. The notch was milled in having a depth of 2 mm, an angle of 45° and a notch radius of 0.25 mm. Uniaxial tensile tests were carried out at room temperature on an Instron 1120 machine according to ISO-527-2 using a crosshead speed of 5 mm/min. The dumb-bell shaped samples were milled from compression moulded plaques having a thickness of 2 mm. For both mechanical tests at least five samples were tested and their results averaged. The samples were dried overnight prior to testing and kept in an exsiccator until the measurement at room temperature was performed.

2.5. Differential scanning calorimetry (DSC)

The crystallisation behaviour of the different blend components was characterised with DSC using a Perkin–Elmer Pyris-1 DSC. The samples were taken from the compression moulded plaques and had a nominal weight of about 6 mg. The samples were heated from − 80 to 290 °C at 10 °C/min, in order to establish the matrix crystallinity present in the compression moulded plaques, isothermally crystallised at 180 °C. The mass matrix crystallinity is calculated from the experimental heat of fusion measured during this first heating run, according to Eq. (1). When a cold crystallisation exotherm on account of the matrix material was present during the first heating run, the crystallisation enthalpy was subtracted from the melt enthalpy

$$X_c = \frac{\Delta H_{m(PET)}}{\Delta H^0_{m(PET,100\%)}} - \frac{|\Delta H_{c(PET)}|}{\Delta H^0_c(T)} w^{-1}_{PET} \times 100\% \quad (1)$$

with X_c, the mass crystallinity, $\Delta H^0_{m(PET,100\%)}$, the heat of fusion of 100% crystalline PET (140.1 J/g from the ATHAS databank), $\Delta H_{m(PET)}$, the melt enthalpy of PET, $|\Delta H_{c(PET)}|/\Delta H^0_c(T)$, (cold) crystallisation enthalpy of PET corrected for the temperature dependence of the crystallisation enthalpy (105.0 J/g) and w_{PET}, the PET weight fraction in the blend.

2.6. Wide angle X-ray diffraction

Wide angle X-ray diffraction (WAXD) measurements were performed using a Rigaku Rotaflex RU-200B rotating anode device. Ni-filtered Cu Kα radiation was used throughout. Diffraction patterns were obtained in the reflection mode, covering the range between 5 and 60° 2θ. Stepscanning involving increments of 0.05° 2θ and fixed time counting (1 min) was applied. The diffracted radiation was registered with a scintillation counter. The samples were pressed directly in a small aluminium mould, according to the previously discussed compression moulding procedure.

3. Results and discussion

3.1. Blend phase morphology and crystallinity of rubber toughened PET

3.1.1. Blend phase morphology of rubber toughened PET

The weight average particle diameters of the examined blend systems are presented in Tables 1–4. A more detailed discussion on the blend phase morphology development and the resulting rheological behaviour has been reported in a previous publication [38]. The binary, non-compatibilised PET/EPR blends display coarse morphologies with large average particle sizes on account of the high interfacial tension and viscosity ratio between the blend components. The maleic anhydride induced compatibilisation reaction only reveals a limited compatibilisation efficiency, resulting in relatively large particle sizes (> 1 μm), not reaching the submicron level (Table 1).

In contrast, the GMA induced compatibilisation reaction is found to be very effective for obtaining a finely sized dispersed phase. Tables 2 and 3 show the strong compatibilisation effect obtained when adding a commercial E–GMA*x* copolymer which has accordingly been proven to be the best compatibilising agent for the PET/EPR blend system. The addition of only a small E–GMA*x* content is sufficient for obtaining submicron sized particles.

Table 1
Weight average particle diameters and notched Izod impact strengths of the PET/(EPR/EPR-*g*-MA) blends as a function of the dispersed phase concentration and composition

Weight fraction of compatibiliser in dispersed phase composition	D_w (μm)	Impact strength (kJ/m^2)
20 wt%		
0	6.45 ± 0.61	2.4 ± 0.3
0.25	3.46 ± 0.36	1.0 ± 0.2
0.75	1.75 ± 0.07	1.2 ± 0.3
1	1.47 ± 0.12	1.0 ± 0.2
30 wt%		
0	9.49 ± 0.91	1.3 ± 0.2
0.25	6.98 ± 0.57	0.8 ± 0.1
0.75	3.39 ± 0.21	1.3 ± 0.5
1	1.82 ± 0.32	1.2 ± 0.2

Further increasing the compatibiliser content in the dispersed phase composition does not lead to a further decrease of the average particle size. Also, increasing the amount of copolymerised GMA from 8 to 12 wt% not necessarily leads to smaller particle sizes. Several reasons can be held responsible for this observation: micelle formation of E–GMA12 in the matrix, higher viscosity of E–GMA12 and crosslinking of the compatibiliser. These factors have been discussed in detail in our previous publication [38].

The crosslinking of the compatibiliser can be the result of two side reactions. Due to the difunctionality of the polyester matrix, this polymer can react at both chain ends, either within one particle or between two different particles. The second crosslinking reaction results from the formation of secondary hydroxyl molecules upon reactive compatibilisation, enabling a crosslinking reaction to take place between the E–GMA*x* compatibiliser chains [38]. This results in the formation of rough, non-spherical morphologies, especially at high concentrations of the compatibiliser. These morphologies cannot be analysed quantitatively.

The addition of directly grafted EPR-*g*-GMA*x* grades to PET/EPR blends is found to be less effective than the use of E–GMA*x* compatibilisers (Table 4) [39]. Although a gradual decrease of D_w is observed with increasing compatibiliser content, especially at a higher dispersed phase concentration, the particle sizes do not reach submicron values. This is accounted for by the high viscosity of the EPR-*g*-GMA*x* grades and the presence of low molar mass GMA containing molecules interfering with the compatibilisation reaction [38].

Fig. 1 presents the phase morphologies of the PET/(EPR/EPR-*g*-GMA*x*) 70/(0/30) blends, for two different EPR-*g*-GMA*x* grades. The EPR-*g*-GMA1.5 blend clearly displays a finer phase morphology and a smaller phase size distribution when compared to the EPR-*g*-GMA2.0 blend. Based on the radical grafting protocol [38], it is believed that the amount

Table 2
Weight average particle diameters and mechanical properties of the PET/(EPR/E–GMA8) blends as a function of the dispersed phase concentration and composition

Weight fraction of compatibiliser in dispersed phase composition	D_w (μm)	Impact strength (kJ/m^2)	Modulus (MPa)	Elongation at break (%)
10 wt%				
0	2.92 ± 0.18	3.2 ± 0.2	2635 ± 182	2.5 ± 1.3
0.1	0.71 ± 0.07	5.1 ± 0.7	2274 ± 23	6.9 ± 1.1
0.25	0.67 ± 0.06	4.2 ± 1.2	2255 ± 59	7.5 ± 1.4
0.4	0.66 ± 0.02	6.7 ± 0.3	2269 ± 80	4.6 ± 0.4
0.75	–	5.0 ± 1.5	2388 ± 100	8.4 ± 1.9
1	–	3.7 ± 0.5	2389 ± 125	2.5 ± 0.4
20 wt%				
0	6.45 ± 0.61	2.4 ± 0.3	1820 ± 69	3.6 ± 0.7
0.1	0.55 ± 0.08	8.3 ± 2.8	1888 ± 57	4.5 ± 0.5
0.25	0.61 ± 0.10	13.6 ± 2.1	1853 ± 65	9.6 ± 1.9
0.4	0.43 ± 0.08	10.6 ± 1.3	1844 ± 87	9.5 ± 3.5
0.75	–	14.0 ± 1.4	1723 ± 120	13.3 ± 1.4
1	–	11.7 ± 2.2	1793 ± 60	37.9 ± 14.5
30 wt%				
0	9.49 ± 0.91	1.3 ± 0.2	1423 ± 114	1.9 ± 0.2
0.1	0.65 ± 0.09	28.8 ± 5.3	1384 ± 59	4.9 ± 1.0
0.25	0.40 ± 0.03	34.3 ± 3.8	1295 ± 66	6.2 ± 0.9
0.4	0.53 ± 0.04	32.2 ± 9.3	1302 ± 18	18.0 ± 4.6
0.75	–	20.5 ± 1.8	1223 ± 72	18.4 ± 5.5
0.9	–	17.3 ± 4.8	1183 ± 56	28.9 ± 13.9
1	–	44.8 ± 13.2	1145 ± 129	4.7 ± 2.4

Table 3
Weight average particle diameters and mechanical properties of the PET/(EPR/E–GMA12) blends as a function of the dispersed phase concentration and composition

Weight fraction of compatibiliser in dispersed phase composition	D_w (μm)	Impact strength (kJ/m^2)	Modulus (MPa)	Elongation at break (%)
10 wt%				
0	2.92 ± 0.18	3.2 ± 0.2	2635 ± 182	2.5 ± 1.3
0.25	1.30 ± 0.17	6.1 ± 1.1	2679 ± 67	1.9 ± 0.2
0.4	–	5.3 ± 0.8	2711 ± 52	1.2 ± 0.4
1	–	5.6 ± 0.6	–	–
20 wt%				
0	6.45 ± 0.61	2.4 ± 0.3	1820 ± 69	3.6 ± 0.7
0.25	0.63 ± 0.06	14.5 ± 0.8	1993 ± 87	2.9 ± 0.3
0.4	–	13.9 ± 0.7	1927 ± 54	2.7 ± 0.3
0.75	–	12.3 ± 2.0	–	–
1	–	13.7 ± 3.6	2004 ± 84	0.8 ± 0.4
30 wt%				
0	9.49 ± 0.91	1.3 ± 0.2	1423 ± 114	1.9 ± 0.2
0.25	0.72 ± 0.11	33.4 ± 1.7	1350 ± 59	3.8 ± 0.1
0.4	0.78 ± 0.05	25.0 ± 3.8	1302 ± 35	4.4 ± 0.4
0.75	–	15.7 ± 1.2	1277 ± 51	5.5 ± 0.5
1	–	22.2 ± 5.4	1278 ± 38	5.0 ± 2.0

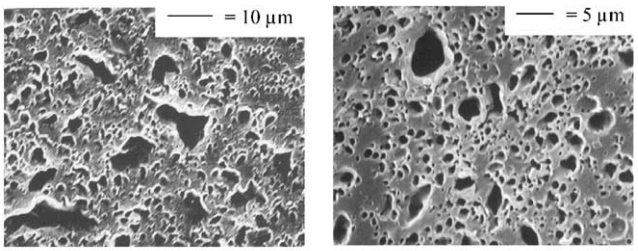

Fig. 1. Blend phase morphology of the 70/(0/30) PET/(EPR/EPR-*g*-GMA*x*) blends with following GMA content: (a) $x = 2.0$ wt% and (b) $x = 1.5$ wt%.

of low molar mass GMA containing molecules is higher in the EPR-*g*-GMA2.0 blend system.

3.1.2. Crystallinity and semicrystalline structure of rubber toughened PET

While the rubber phase dispersion and the interfacial interaction with the matrix phase are dominant parameters determining the mechanical behaviour, it should be kept in mind that the investigated PET matrix is semicrystalline. Table 5 presents the melting enthalpies and melting temperatures associated with the first heating endothermic transition of the PET/(EPR/E–GMA8) and the

Table 4
Weight average particle diameters and mechanical properties of the PET/(EPR/EPR-*g*-GMA1.5) blends as a function of the dispersed phase concentration and composition

Weight fraction of compatibiliser in dispersed phase composition	D_w (μm)	Impact strength (kJ/m^2)	Modulus (MPa)	Elongation at break (%)
10 wt%				
0	2.92 ± 0.18	3.2 ± 0.2	2635 ± 182	2.5 ± 1.3
0.25	1.05 ± 0.08	4.8 ± 1.0	2628 ± 2	1.5 ± 0.2
0.75	1.30 ± 0.17	4.3 ± 0.9	–	–
1	2.00 ± 0.25	4.2 ± 0.5	–	–
20 wt%				
0	6.45 ± 0.61	2.4 ± 0.3	1820 ± 69	3.6 ± 0.7
1	1.54 ± 0.28	5.9 ± 2.5	1870 ± 28	1.9 ± 0.2
30 wt%				
0	9.49 ± 0.91	1.3 ± 0.2	1423 ± 114	1.9 ± 0.2
0.25	3.77 ± 0.23	2.8 ± 0.5	1155 ± 57	2.7 ± 0.4
0.75	1.52 ± 0.17	11.1 ± 1.5	–	–
1	1.13 ± 0.18	19.8 ± 8.5	1252 ± 53	3.0 ± 0.2

PET/(EPR/E–GMA12) blends, both displaying submicron dispersed phase sizes. The results of this first heating run reflect the crystalline state present in the moulded sample, which is affected by the thermal and mechanical history imposed during the moulding process.

Fig. 2(a) shows the first heating endothermic curves of the $70/(x/y)$ compositions of the PET/(EPR/E–GMA8) blend at high temperatures. A typical double melting behaviour characteristic for the PET matrix can be observed, illustrating the recrystallisation process of thin, less perfect crystals formed during the isothermal compression moulding procedure at 180 °C. The lower peak melting temperatures are located in the vicinity of the T_m of pure PET (242.6 °C). The T_m values of the $70/(x/y)$ E–GMA8 blends are slightly lower. The blends do not display any cold crystallisation, whereas pure PET samples can reveal a small cold crystallisation peak around 133 °C.

From Table 5 it can be seen that both the E–GMA8 and the E–GMA12 compatibilised blends display heat of fusion values (ΔH_m) similar or higher when compared to that of pure, semicrystalline PET, prepared under the same compression moulding procedure. The E–GMA8 compatibilised blends with a higher dispersed phase concentration display higher heat of fusions, independent of the dispersed phase composition. Various authors [29,34,40–41] have reported on increased crystallinities in rubber modified systems and attributed the increase to a nucleating activity of the matrix/rubber interface. For our investigated rubber modified PET systems, a nucleating activity of the dispersed phase could not be established unambiguously.

A shift towards a higher fraction of the lower melting peak can be observed with increasing E–GMA8 content in the dispersed phase composition, accompanied by a decrease of the matrix crystallinity. This effect is believed to originate from interfacial reactions taking place upon reactive compatibilisation and the occurrence of the earlier described crosslinking reactions [38]. This will inevitably interfere with the crystallisation process, whereby it is believed that the increased interaction with the compatibiliser hinders the process of recrystallisation and crystal growth. Such effect has been reported by Oshinski et al. [10] for nylon6/SEBS-*g*-MA blends, by Papadopoulou and Kalfoglou [42] for PET/PP blends compatibilised with SEBS-*g*-MA, and by Martuscelli [43] who studied various blend systems and stated that increased viscosities upon reactive compatibilisation can cause a decrease of the crystallisation rate. The E–GMA12 compatibilised blends basically display the same trends as observed for the E–GMA8 modified blends.

The DSC thermographs presented in Fig. 2(b) reveal the presence of a second, small endothermic peak at a temperature of approximately 90 °C. This melting peak is identified to originate from the E–GMA*x* compatibilising agent. The compatibilisers are thus found to crystallise at the applied moulding conditions. The crystallinities as well as the melting and crystallisation temperatures of the

Table 5
First heating endothermic DSC results of PET in the PET/(EPR/E–GMA8) and PET/(EPR/E–GMA12) blends

Weight fraction compatibiliser in dispersed phase	PET/(EPR/E–GMA8)			PET/(EPR/E–GMA12)		
	ΔH_m (J/g PET)	T_m, Peak (°C)	X_c (%)	ΔH_m (J/g PET)	T_m, Peak (°C)	X_c (%)
PET	33.0 ± 2.3	242.6	23.5	33.0 ± 2.3	242.6	23.5
10 wt%						
0	35.0	242.7	25.0	35.0	242.7	25.0
0.25	35.4	242.8	25.3	30.7	242.9	21.9
0.4	35.8	242.0	25.6	36.3	242.4	25.9
0.75	33.8	241.9	24.2	–	–	–
1	33.3	240.5	23.8	41.0	241.8	29.3
20 wt%						
0	40.6	243.4	29.0	40.6	243.4	29.0
0.1	38.1	243.2	27.2	–	–	–
0.25	32.8	242.1	23.4	37.0	243.2	26.4
0.4	35.7	242.6	25.5	27.5	239.7	21.4
0.75	29.6	241.6	21.1	30.4	242.1	21.7
1	28.8	240.6	20.6	28.8	–	20.6
30 wt%						
0	43.7	237.9	31.2	43.7	237.9	31.2
0.1	47.7	238.8	34.1	–	–	–
0.25	44.4	237.5	31.7	36.8	243.2	26.3
0.4	44.0	239.7	31.4	34.5	241.2	24.7
0.75	43.8	240.2	31.3	40.4	241.4	28.8
0.9	38.9	240.9	27.8	–	–	–
1	34.0	240.1	24.3	–	–	–

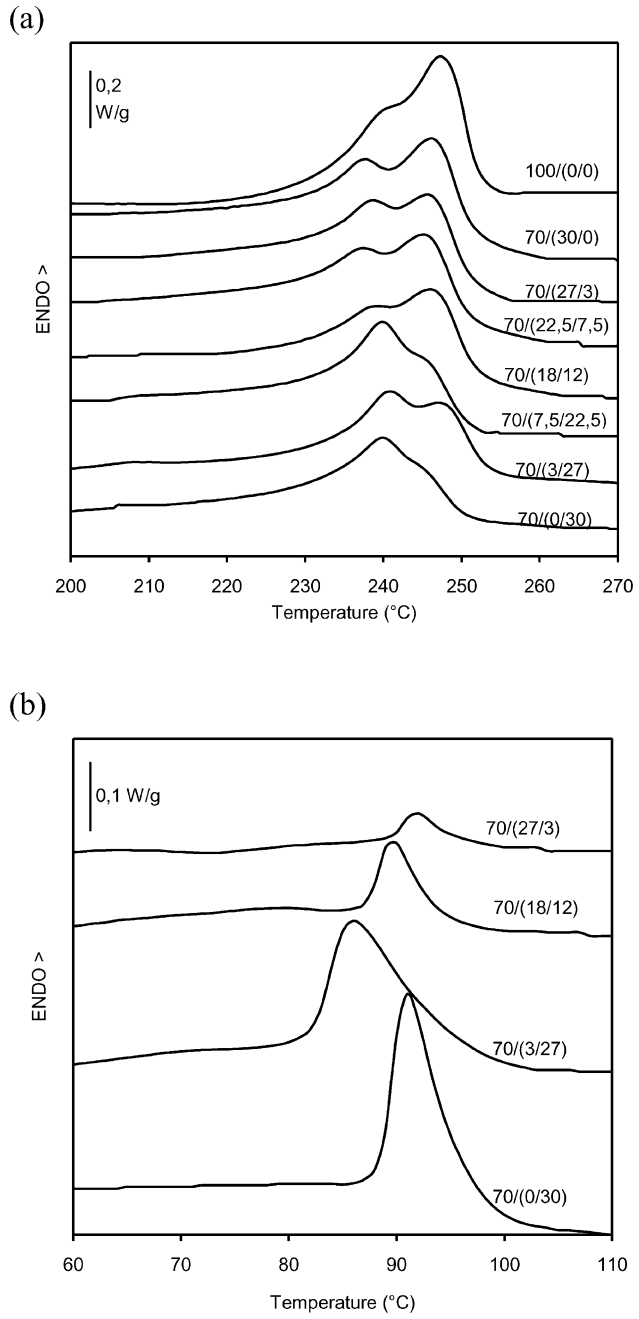

Fig. 2. DSC first heating endotherms of the PET/(EPR/E–GMA8) $70/(x/y)$ blends for various dispersed phase compositions (a) melting endotherms of PET; (b) melting endotherms of E–GMA8.

E–GMAx component in the blends are lower than those of the pure E–GMAx copolymer. This indicates that their crystallisation is hindered by the presence of EPR and the interfacial interaction with the PET matrix. The EPR rubber component only slightly crystallises in the total absence of E–GMAx; otherwise, no melting peak could be observed.

WAXD measurements were performed on the pure components and several of the PET/(EPR/E–GMA8) blends, in order to assess the influence of the rubber dispersion and reactive compatibilisation on the crystal

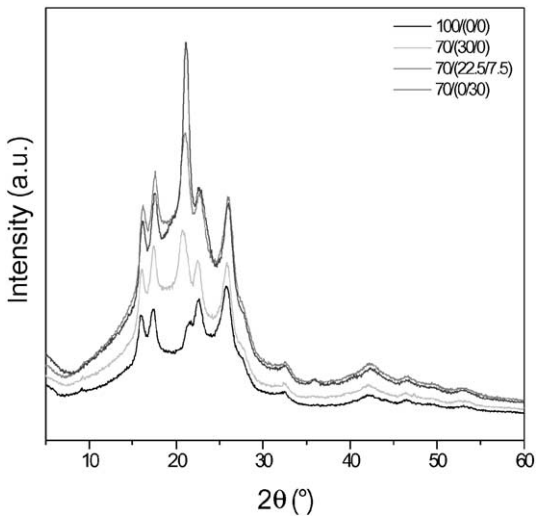

Fig. 3. WAXD spectra of the PET/(EPR/E–GMA8) $70/(x/y)$ blends for various dispersed phase compositions.

structure (Fig. 3). The ethylene sequences clearly display two major reflections at 21.15 and 23.5°, revealing the presence of crystalline E–GMA8 in the examined blends. The remaining reflections originate from the semicrystalline PET matrix. The PET reflections do not change due to the addition of the dispersed phase components and essentially remain located at the same 2θ values. The PET/EPR 70/30 blend shows minor reflection of the ethylene sequences of EPR, indicating the slight crystallinity of the elastomer in the binary blend, as already observed with DSC. Integration of the spectra is difficult due to the presence of the two different crystalline materials and therefore the PET crystallinity in the blends could not be assessed using WAXD.

3.2. Notched impact behaviour of rubber toughened PET

The toughening ability of the various elastomeric dispersed phases is evaluated by notched Izod impact strength measurements at room temperature. The impact strength of pure semicrystalline PET was established at 2.5 ± 0.1 kJ/m^2. The samples clearly fractured in a brittle manner, displaying only a microscopically sized stress whitened zone and a complete separation of the sample halves [1,44].

The non-compatibilised PET/EPR blends do not display any improvement of the impact strength. This is caused by the high degree of incompatibility between both blend components, leading to large particle sizes without any significant interfacial adhesion.

3.2.1. Maleic anhydride compatibilised PET/elastomer blends

The notched Izod impact strengths of the PET/(EPR/EPR-g-MA) blends are summarised in Table 1. They are reported as a function of the dispersed phase

concentration and the compatibiliser content within the dispersed phase. Gradual replacement of EPR with EPR-*g*-MA does not result in any improvement of the impact strength at the examined dispersed phase concentrations and compositions. In fact, the impact strengths are even lower compared to that of pure PET. Hence, these maleated blend systems are unable to provide any significant toughness improvement of the PET matrix.

3.2.2. Glycidyl methacrylate compatibilised PET/elastomer blends

The impact strengths of the blends based on the home-made EPR-*g*-GMA*x* grades are presented in Fig. 4. It is obvious that both compatibilised blend systems display a completely different impact response. No significant improvement of the impact toughness can be observed upon the addition of EPR-*g*-GMA2.0 to the PET/EPR blends, at any of the examined dispersed phase concentrations or compositions. On the other hand, the PET/EPR blends compatibilised with EPR-*g*-GMA1.5 show improved impact strengths at a dispersed phase concentration of 30 wt% (Fig. 4 and Table 4). Gradually increasing the EPR-*g*-GMA1.5 content leads to an increase of the impact strength and interestingly, a gradual decrease of the particle size (Table 4). The highest impact strength is obtained for the binary 70/(0/30) PET/(EPR/EPR-*g*-GMA1.5) blend, failing in a semiductile manner. This is commonly accompanied by a large standard deviation, as can be observed from Fig. 4. The $90/(x/y)$ and $80/(x/y)$ blends show no significant improvement and fail in a brittle manner.

Tables 2 and 3 summarise the notched Izod impact strengths of the PET/(EPR/E–GMA8) and the PET/(EPR/E–GMA12) blends, respectively. Figs. 5 and 6 present the

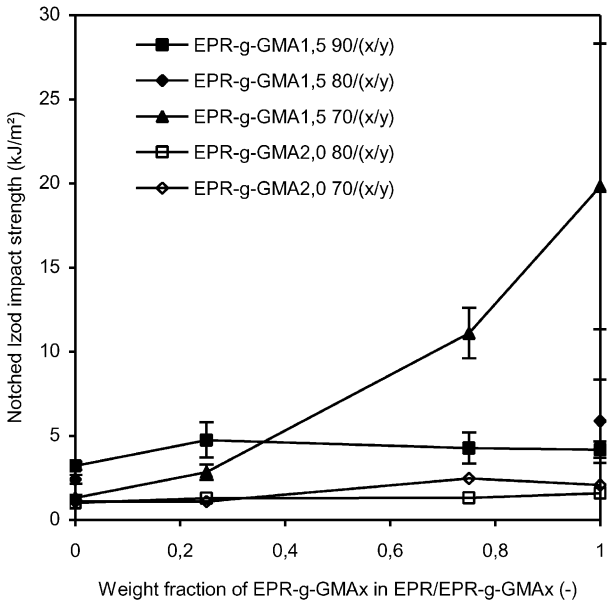

Fig. 4. Notched Izod impact strength of the PET/(EPR/EPR-*g*-GMA*x*) blends as a function of the EPR-*g*-GMA*x* fraction in the dispersed phase for the two home-made EPR-*g*-GMA*x* grades.

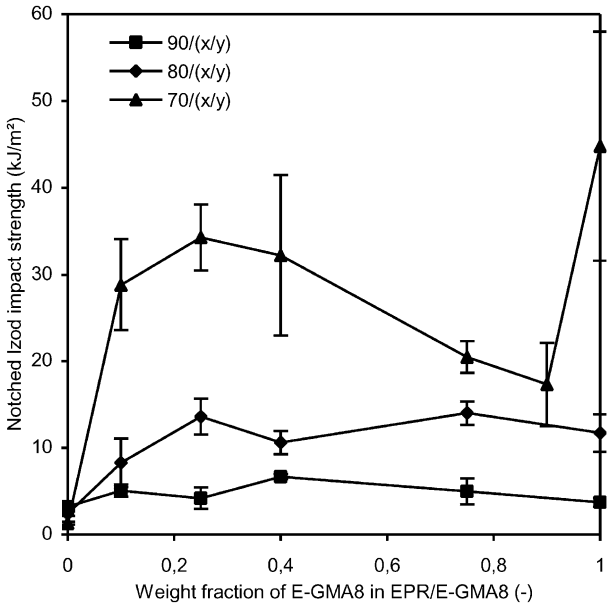

Fig. 5. Notched Izod impact strength of the PET/(EPR/E–GMA8) blends as a function of the weight fraction of E–GMA8 in the dispersed phase.

impact strengths as a function of the dispersed phase composition for the different dispersed phase concentrations. We first consider the impact response of the PET/(EPR/E–GMA8) blend system. A minimum dispersed phase concentration of 30 wt% is needed to induce a brittle–ductile transition of the fracture mode. Only the $70/(x/y)$ blends break in a ductile manner, showing extensive stress whitening and a distorted shape of the fracture plane. The presence of only a small amount of E–GMA8 is found to be very effective for obtaining a strong improvement of the impact strength when the dispersed phase concentration is high. Increasing the E–GMA8 content within a constant dispersed phase concentration only leads to a small further increase of the impact strength, regardless of the dispersed phase concentration. The $70/(x/y)$ blends display a marked drop of the impact strength and a semiductile fracture mode when the E–GMA8 content in the dispersed phase is high (>50 wt%). A remarkable result, however, is observed for the 70/(0/30) PET/(EPR/E–GMA8) blend. This blend composition displays a very high impact strength and a ductile fracture mode, exhibiting extensive stress whitening.

In general, the PET/(EPR/E–GMA12) blends display similar trends as observed for the E–GMA8 compatibilised blends (Fig. 6). A minimum dispersed phase concentration of 30 wt% is necessary to induce a ductile fracture mode whereby a small amount of compatibiliser is sufficient for highly improved impact strengths. Further increasing the E–GMA12 content is seen to deteriorate the impact toughness. The E–GMA12 content in the dispersed phase composition does not greatly influence the impact strength of the $90/(x/y)$ and the $80/(x/y)$ blends. The PET/(EPR/E–GMA12) 70/(0/30) blend also displays a high impact

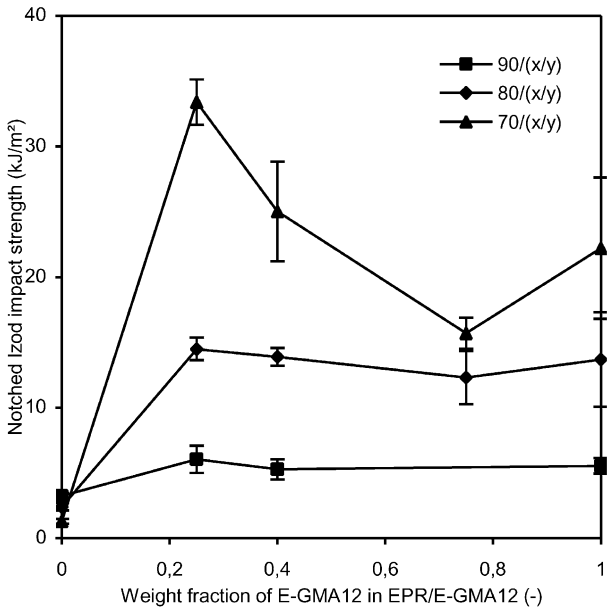

Fig. 6. Notched Izod impact strength of the PET/(EPR/E–GMA12) blends as a function of the weight fraction of E–GMA12 in the dispersed phase.

strength, similar to that of the E–GMA8 blend. In general, it can be seen that the impact strengths of the PET/(EPR/E–GMA12) blend system are lower than those obtained for the PET/(EPR/E–GMA8) blends.

3.2.3. Correlation between the blend characteristics and the impact behaviour

In order to understand the observed notched impact response, both the morphological characteristics as well as the structural blend features need to be taken into consideration.

Fig. 7 presents the notched Izod impact strength as a function of the weight average particle diameter for all examined blend systems. The impact strength can be seen to increase with a decreasing particle size. However, it also becomes clear that although several compositions have small particle diameters, they do not exhibit a high impact toughness. This indicates that besides the average particle size also the dispersed phase concentration (i.e. the number of dispersed particles) is very important. For many rubber modified notch sensitive matrices, it could be established that the brittle–ductile transition occurred at a critical value of the interparticle distance [4,8,12,37]. The interparticle distance needs to be lower than a critical value (IDc) in order to induce a ductile fracture mode. The interparticle distance is defined as the matrix ligament thickness between two adjacent rubber particles, according to the following equation

$$\mathrm{ID} = D\left[\left(\frac{\pi}{6\phi_r}\right)^{1/3} - 1\right] \quad (2)$$

with D, the dispersed phase particle diameter, ID, the interparticle distance and ϕ_r, the rubber volume concentration. The dependence of the impact strength on the interparticle distance, as calculated from the morphological analysis according to Eq. (2), is presented in Fig. 8 for all studied blend systems.

The maleated blend systems were found to display relatively high dispersed phase particle sizes and low impact strengths. The interparticle distances of the PET/(EPR/EPR-*g*-MA) blends are apparently too high in order to reach their critical value (Fig. 8). The material is subsequently unable to induce an overall deformation mechanism and a brittle–ductile transition of the fracture mode. It is not possible to provide a numerical estimation of the IDc for the examined

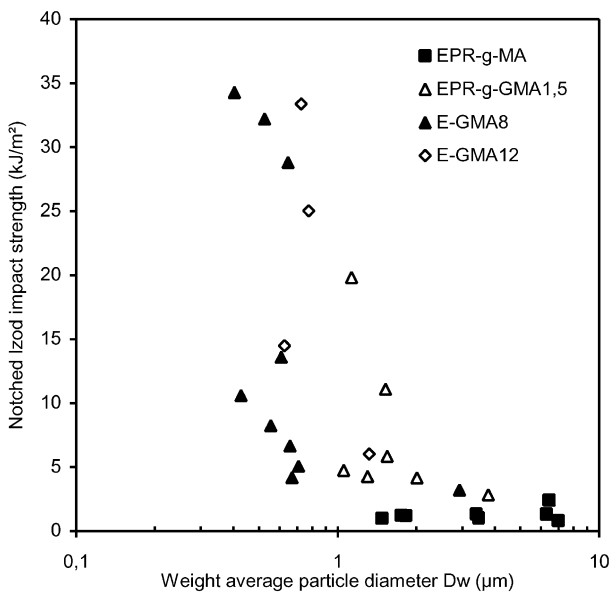

Fig. 7. Notched Izod impact strength as a function of the dispersed phase particle size for the various rubber modified PET systems.

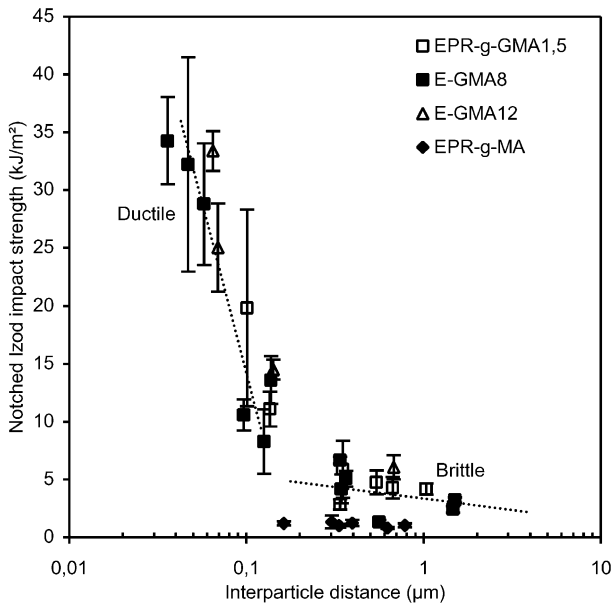

Fig. 8. Notched Izod impact strength as a function of the interparticle distance for the various rubber modified PET systems.

PET/(EPR/EPR-*g*-MA) blends, as this value could not be determined from the experimental results. It can be concluded that the inability of the maleic anhydride compatibilisation reaction to generate fine phase dispersions is the main reason for the lack of impact toughening. It is important to note that the IDc is not necessarily the same for every dispersed phase [7,15]. For PBT/EPR-*g*-MA and PBT/SEBS-*g*-MA blends, two different IDcs were found [7].

The EPR-*g*-GMA1.5 compatibilised blends also did not display submicron sized particle diameters. A few PET/(EPR/EPR-*g*-GMA1.5) blends did, however, display a semi-ductile impact behaviour. From Fig. 8 it can be seen that their respective interparticle distances are located in the vicinity of an apparent critical value. The combination of fairly low particles sizes ($D_w \approx 1$ μm) and a high dispersed phase concentration makes these blends susceptible for reaching higher impact strengths. As stated earlier, the blends based on the EPR-*g*-GMA2.0 compatibiliser displayed rougher morphologies and bigger particles (Fig. 1). The impact response clearly revealed that this is detrimental for reaching a satisfying toughness improvement (Fig. 4).

It has been proven that the strongest improvement of the impact strength is obtained for the PET/(EPR/E–GMA*x*) blend systems, whereby a minimum dispersed phase concentration of 30 wt% is needed to induce a brittle–ductile transition of the fracture mode. Fig. 7 and Tables 2–3 show that although several compositions of the E–GMA8 and E–GMA12 compatibilised blends have low particle sizes, they lack the ability to provide a high toughness. Based on Fig. 8, it becomes clear that only the 30 wt% rubber blends display interparticle distances below an apparent critical value. The combination of small particle sizes and a high dispersed phase concentration results in the low interparticle distances and, as a consequence, in a ductile fracture mode and a strongly improved toughness. The lower impact strengths observed for the PET/(EPR/E–GMA12) blends compared with those of the E–GMA8 compatibilised blends can be attributed to the larger particle sizes of the former.

From the results summarised in Fig. 8, it can be clearly seen that the various GMA compatibilised PET/EPR blends display the same IDc which can be established experimentally at approximately 0.1 μm. Below this IDc, the impact strength increases with decreasing interparticle distance. The IDc is not influenced by the content of functional groups, the way of incorporation (grafting or copolymerisation) and the nature of the elastomeric compatibiliser. Kanai et al. [7], Borggreve and Gaymans [14] and Wu [37] also found that the amount of grafted functionalities did not significantly affect the IDc. Although the E–GMA*x* components have a higher modulus when compared to EPR, this does not seem to be important when the E–GMA*x* content remains low. Using Eq. (2) and the IDc value of 0.1 μm, critical particle sizes of 0.19, 0.44 and 1.1 μm can be calculated for rubber concentrations of 10, 20 and 30 wt%, respectively. Tables 2 and 3 show that the $70/(x/y)$ compositions clearly have particle sizes far below the respective limit and several $80/(x/y)$ blends reveal particle sizes approaching the limit needed for a ductile behaviour.

The PET/(EPR/E–GMA*x*) blends having a high E–GMA*x* content have not been considered up to now since they could not be analysed quantitatively as a result of their irregular shaped morphologies. In general, they display inferior impact strengths and a brittle or semiductile fracture mode. Several factors can be held responsible for this impact response. The most important factor is the occurrence of the earlier discussed crosslinking reactions [38]. The difunctionality of PET can lead to a reaction at both chain ends. This consequently increases the overall blend viscosity. The PET chain flexibility will be hindered causing a higher resistance towards chain movement and a shear yielding deformation mechanism. In addition, the E–GMA*x* compatibilisers display higher *E*-moduli when compared to EPR. Dispersed phases having a higher *E*-modulus are known to be less effective for the toughening of nylon6 as cavitation becomes more difficult [15]. The stiffness of the dispersed EPR/E–GMA*x* phase can increase further due to the occurrence of the proposed crosslinking reactions, leading to a network of compatibiliser chains. Moreover, it is not unlikely that the irregular shape of the dispersed phase influences the stress state in the matrix surrounding the dispersed phase particles, causing unfavourable conditions for a multiple deformation mechanism to occur.

The GMA induced interfacial reaction also results in an increased adhesion between the PET matrix and the dispersed phase. However, there does not seem to exist a clear correlation between the concentration of (copolymerised or grafted) GMA functionalities and the resulting

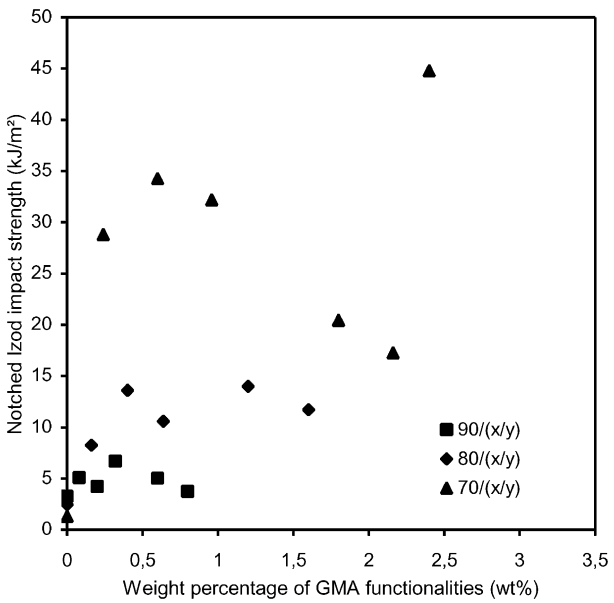

Fig. 9. Notched Izod impact strength of the PET/(EPR/E–GMA8) blends as a function of the GMA concentration in the blend.

impact strengths when assuming that a higher initial GMA concentration leads to a higher amount of matrix coupling at the interface (Fig. 9). Borggreve and Gaymans [14] reported that for nylon/rubber blends the initial MA concentration as well as the amount of nylon grafted at the interface, which increased with the initial MA content, had no influence on the impact behaviour of the blends.

3.3. Tensile properties of glycidyl methacrylate compatibilised rubber toughened PET

The tensile properties of the different GMA compatibilised blends have been established using uniaxial tensile testing. Pure, semicrystalline PET has an *E*-modulus of 2800 ± 200 MPa and a high yield stress of 140 ± 15 MPa on account of the relatively high degree of crystallinity of PET in the samples. The yield stress and modulus are known to increase with an increasing degree of crystallinity [1]. The main problem encountered when performing tensile tests on semicrystalline PET is the formation of a stable neck upon yielding. Geometrical instabilities and the presence of impurities are found to be highly unfavourable for the stability of the propagating neck. The latter is most likely the main reason for the different elongations at break obtained for pure PET. Over a range of 12 samples, various broke directly after reaching the yield point ($\varepsilon_b = 6–7\%$). Others reached reasonable propagations of the neck during the subsequent cold drawing stage (between 15 and 45%), and some samples even deformed up to 200%. Hence, several samples exhibited a ductile tensile fracture ($\varepsilon_b > 10\%$) [45] whereas others could not. No average value of the ultimate elongation of pure PET will therefore be provided.

The main tensile properties of the PET/(EPR/E–GMA8), PET/(EPR/E–GMA12) and PET/(EPR/EPR-*g*-GMA1.5) blends are summarised in Tables 2, 3 and 4, respectively. The non-compatibilised PET/EPR blends display very low ε_b values due to their coarse phase morphologies and lack of interfacial interaction with PET. This inevitably leads to debonding and premature rupture, often observed for non-compatibilised systems [46,47]. The addition of an effective compatibiliser finely disperses the rubber particles in the PET matrix and leads to an increased interface across which grafting can occur. Of the examined blend systems, only the E–GMA8 compatibilised blends were found to display reasonable elongations at break. Fig. 10 presents the ε_b values of the PET/(EPR/E–GMA8) blends as a function of the dispersed phase composition and concentration.

At low E–GMA8 contents (<40 wt%), the ultimate elongations are located close together. Upon increasing the E–GMA8 content, an increase of the elongations at break can be observed, whereby higher dispersed phase concentrated blends display higher ε_b values. Hence, despite the irregular shaped phase morphologies at high E–GMA8 contents, the ε_b values keep on rising. The compatibilisation reaction and the formation of crosslinks lead to an increase of interfacial interactions and the interface strength,

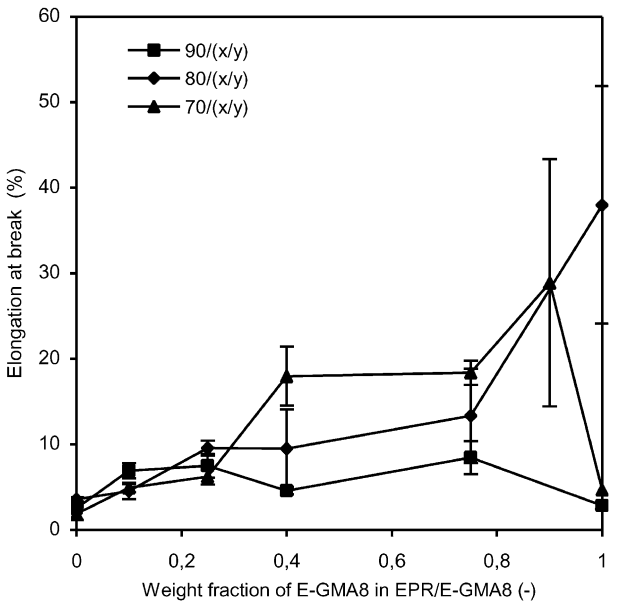

Fig. 10. Elongation at break for the PET/(EPR/E–GMA8) blends as a function of the weight fraction of E–GMA8 in the dispersed phase.

consequently increasing the adhesion. The influence of the interfacial adhesion becomes clear from Fig. 11. It can be seen that a higher content of GMA functionalities present leads to higher elongations at break, regardless of the concentration and the composition of the dispersed phase. A more comprehensive view is provided by Fig. 12 presenting the effect of both the GMA concentration and the matrix crystallinity on the ε_b values. It becomes clear that increasing the GMA concentration increases the elongations at break. From Fig. 12 and Tables 2 and 3, we may conclude that the effect of the GMA functionality concentration prevails over the effect of the matrix crystallinity. When

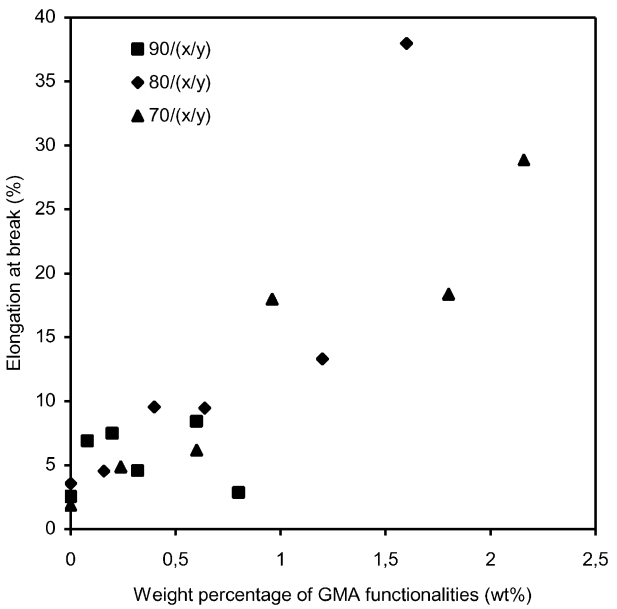

Fig. 11. Elongation at break for the PET/(EPR/E–GMA8) blends as a function of the GMA concentration in the blend.

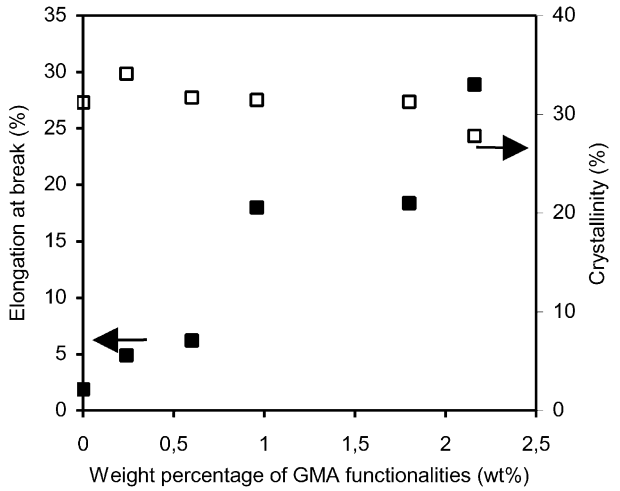

Fig. 12. Elongation at break (■) and PET matrix crystallinity (□) as a function of the GMA concentration in the blend for the $70/(x/y)$ compositions of the PET/(EPR/E–GMA8) blends.

increasing the GMA concentrations from 0.5 to 2 wt%, a steep increase of the elongation at break can be observed whereas the crystallinity hardly changes. The same effect is observed for the other dispersed phase concentrations. Hence, the improved ε_b values upon the addition of E–GMA8 result from an increased coupling of PET at the interface due to the reactive compatibilisation and the crosslinking reactions.

Peel strength tests performed by Champagne [48] reported that the adhesion between GMA copolymers and PET depends strongly on the copolymer structure. It was found that a high GMA content not necessarily leads to a stronger adhesion, providing an explanation for the lower elongations at break observed for the E–GMA12 compatibilised blends, although it needs to be taken into account that the possible formation of E–GMA12 micelles may also interfere with the mechanical properties. The low ε_b values of the EPR-*g*-GMA1.5 blends are most likely caused by the relatively low content of grafted GMA groups (1.5 wt%) and the interference of low molar mass GMA molecules during reactive compatibilisation.

The *E*-modulus of the blends is found to decrease with increasing dispersed phase concentration, as could be expected upon the dispersion of a rubbery phase [15]. Fig. 13(a) presents the normalised *E*-moduli (E_{blend}/E_{PET}) as a function of the rubber volume concentration for the different GMA compatibilised blends (compatibiliser content = 25 wt%). The modulus displays an almost linear decrease with increasing dispersed phase concentration. The E–GMA12 blends generally have a higher modulus compared to the E–GMA8 compatibilised blends. The influence of the EPR/compatibiliser ratio could not be established unambiguously. The dependence of the yield stress on the rubber volume concentration is investigated for the PET/(EPR/E–GMA8) blends (Fig. 13(b)). The yield stress is found to decrease with increasing dispersed phase concentration, but still remains high due to the semicrystalline nature of the PET matrix.

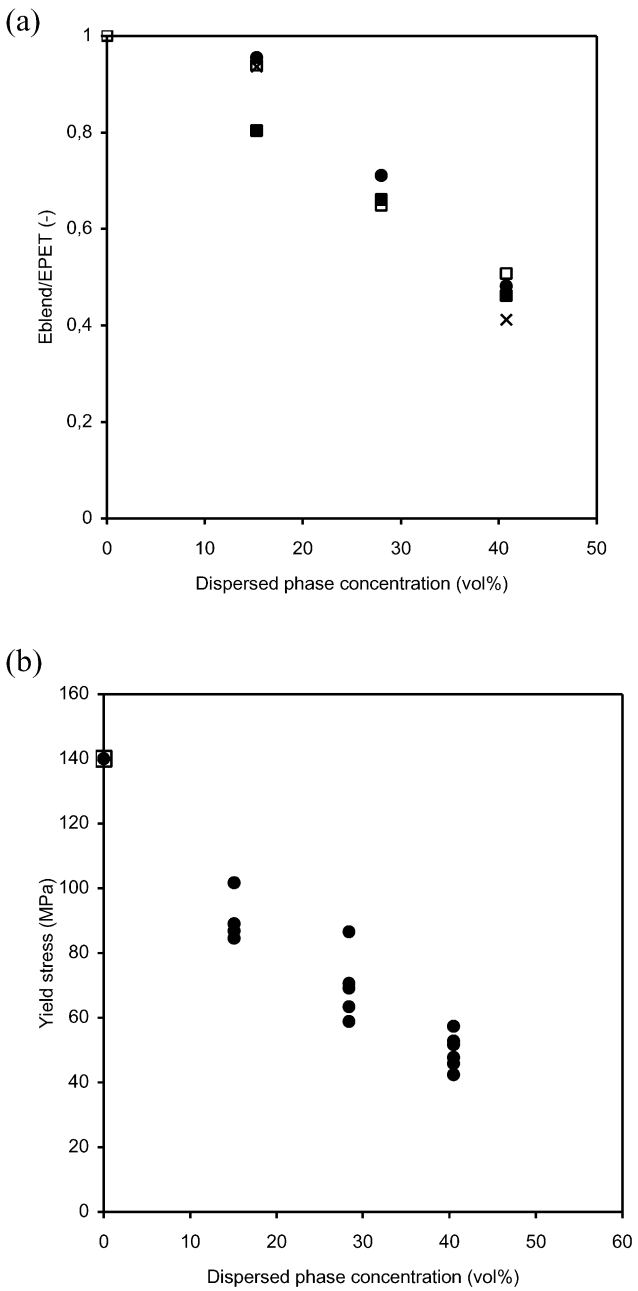

Fig. 13. (a) Relative *E*-moduli of the GMA compatibilised rubber toughened PET systems as a function of the dispersed phase concentration, having a compatibiliser content of 25 wt% ((□) EPR, (■) E–GMA8, (◇) E–GMA12, (●) and (×) EPR-*g*-GMA1.5). (b) Yield stress of the PET/(EPR/E–GMA8) blends as a function of the dispersed phase concentration.

4. Conclusions

A comparative study regarding the toughening efficiency of various elastomeric modifiers with respect to the impact toughening of semicrystalline PET is presented. The

investigated maleic anhydride compatibilised blends displayed almost no increase of the impact strength, whereas the GMA compatibilised blends revealed a pronounced improvement of the impact toughness. The most effective toughening route of semicrystalline PET is provided by a dispersed phase consisting of a preblend of an EPR elastomer and an E–GMA*x* compatibiliser.

The impact behaviour of rubber toughened PET is clearly found to be primarily controlled by the morphological characteristics of the dispersed phase. The interparticle distance plays a very crucial role. IDc is established experimentally at 0.1 μm, being identical for the different GMA compatibilised blend systems. This IDc appears to be independent of the amount of GMA functionalities present, the way of incorporation in the chain (grafting or copolymerisation) and the nature of the compatibiliser. The inability of the MA induced compatibilisation reaction to generate fine phase morphologies is the main reason for the lack of impact toughening. A high content of the E–GMA*x* compatibiliser is generally unfavourable on account of the irregular shaped morphologies due to crosslinking, and the lower elastomeric nature of E–GMA*x*.

The dispersion of the rubbery phase decreases the elastic modulus and the yield strength. The ultimate elongation at break is highly sensitive to the amount of adhesion present at the interface, whereby the E–GMA8 compatibilised blends displayed the highest elongations at break.

Based on the fine dispersed phase morphologies, the highly improved impact toughness, the ductile fracture mode and the tensile properties, we may conclude that the ternary PET/(EPR/E–GMA8) blends provide the best toughening route for semicrystalline PET. A high dispersed phase concentration (30 wt%) and a low E–GMA8 content in the dispersed phase (<50 wt%) form the basic requirements.

Acknowledgments

The authors are indebted to the IWT-Belgium for a grant to one of them (W. Loyens) and to the Kuleuven Research Council for financial support of the laboratory (GOA)blend project 98/06.

References

[1] Gaymans RJ. In: Paul DR, Bucknall CB, editors. Polymer blends: performance, vol. 2. New York: Wiley; 2000. chapter 25.
[2] Wu S. Polymer international 1992;29:229–47.
[3] Bucknall CB. Toughened plastics. Essex: Applied Science Publishers; 1979.
[4] Bucknall CB. In: Paul DR, Bucknall CB, editors. Polymer blends: performance, vol. 2. New York: Wiley; 2000. chapter 22.
[5] Hourston DJ, Lane S. In: Collyer AA, editor. Rubber toughened polymers. Cambridge: Chapman & Hall; 1994. chapter 8.
[6] Groeninckx G, Dompas D. In: Araki T, Tran-Cong Q, Shibayama M, editors. Structure and properties of multiphase polymeric materials. New York: Marcel Dekker; 1998. chapter 12.
[7] Kanai H, Sullivan V, Auerbach A. J Appl Polym Sci 1994;53:527–41.
[8] Sanchez-Solis A, Estrada MR, Cruz J, Manero O. Polym Engng Sci 2000;40(5):1216–25.
[9] Wu S. Polym Engng Sci 1987;27:335–43.
[10] Oshinski AJ, Keskkula H, Paul DR. Polymer 1992;33(2):268–83.
[11] Oshinski AJ, Keskkula H, Paul DR. Polymer 1992;33(2):284–93.
[12] Borggreve RJM, Gaymans RJ, Schijer J, Ingen Housz JF. Polymer 1987;28:1489–96.
[13] Van der Wal A, Nijhof R, Gaymans RJ. Polymer 1998;39:6031–44.
[14] Borggreve RJM, Gaymans RJ. Polymer 1989;30:63–70.
[15] Borggreve RJM, Gaymans RJ, Schuijer J. Polymer 1989;30:71–7.
[16] Oshinski AJ, Keskkula H, Paul DR. Polymer 1996;37(22):4909–18.
[17] Dijkstra K, Gaymans RJ. Polymer 1994;35(2):332–5.
[18] Hale W, Lee J-H, Keskkula H, Paul DR. Polymer 1999;40:3621–9.
[19] Van der Wal A, Mulder JJ, Oderkerk J, Gaymans RJ. Polymer 1998; 39(26):6781–7.
[20] Dompas D, Groeninckx G. Polymer 1994;35(22):4743–9.
[21] Dompas D, Groeninckx G, Isogawa M, Hasegawa T, Kadokura M. Polymer 1994;35(22):4750–9.
[22] Dompas D, Groeninckx G, Isogawa M, Hasegawa T, Kadokura M. Polymer 1994;35(22):4760–5.
[23] Hobbs SY, Dekkers MEJ, Watkins VH. J Mater Sci 1988;23: 1219–24.
[24] Dekkers MEJ, Hobbs SY, Watkins VH. J Mater Sci 1988;23: 1225–30.
[25] Brady AJ, Keskkula H, Paul DR. Polymer 1994;35(17):3665–72.
[26] Abu-Isa IA, Jaynes CB, O'Gara JF. J Appl Polym Sci 1996;59: 1957–71.
[27] Cook WD, Zhang T, Moad G, Van Deipen G, Cser F, Fox B, O'Shea M. J Appl Polym Sci 1996;62:1699–708.
[28] Hage E, Hale W, Keskkula H, Paul DR. Polymer 1997;38(13): 3237–50.
[29] Hale W, Keskkula H, Paul DR. Polymer 1999;40:3353–65.
[30] Hale W, Pessan LA, Keskkula H, Paul DR. Polymer 1999;40: 4237–50.
[31] Cecere A, Greco R, Ragosta G, Scarzini G, Tagliatela A. Polymer 1990;31:1239–44.
[32] Akkapeddi MK, Van Buskirk B, Mason CD, Chung SS, Swamikannu X. Polym Engng Sci 1995;35(1):72–8.
[33] Penco M, Pastorino MA, Ochiello E, Garbassi F, Braglia R, Giannotta G. J Appl Polym Sci 1995;57:329–34.
[34] Mouzakis DE, Papke N, Wu JS, Karger-Kocsis J. J Appl Polym Sci 2001;79:842–52.
[35] Tanrattanakul V, Hiltner A, Baer E, Perkins WG, Massey FL, Moet A. Polymer 1997;38(9):2191–200.
[36] Hert M. Angew Macromol Chem 1992;196(3377):89–99.
[37] Wu S. Polymer 1985;26:1855–63.
[38] Loyens W, Groeninckx G. Macromol Chem Phys 2002;203(10/11): 1702–15.
[39] Majumdar B, Paul DR. In: Paul DR, Bucknall CB, editors. Polymer blends: formulation, vol. 1. New York: Wiley; 2000. chapter 17.
[40] Jha A, Bhowmick AK. Polymer 1997;38(17):4337–44.
[41] Kalfoglou NK, Skafida DS, Kallitsis JK. Polymer 1997;37(15): 3387–95.
[42] Papadopoulou CP, Kalfoglou NK. Polymer 2000;41:2543–55.
[43] Martuscelli E. Polym Engng Sci 1984;24(8):563–86.
[44] Vu-Khanh T. Polymer 1988;29:1979–84.
[45] Ward IM. In: Ward IM, Hadley DW, editors. Mechanical properties of solid polymers. New York: Wiley; 1993.
[46] Greco R, Malinconico M, Martuscelli E, Ragosta G, Scarzini G. Polymer 1987;28:1185–9.
[47] Carté TL, Moet A. J Appl Polym Sci 1991;48:611–24.
[48] Champagne MF. Proceedings of the International Symposium on Polymer Blends and Alloys: Polyblends'99, Montreal, Canada; 1999. p. 37.